Understanding the strain rate sensitivity of nanocrystalline copper using molecular dynamics simulations

Ali Rida, M. Micoulaut, Emmanuelle Rouhaud, Ali Makke

Version of Record: https://www.sciencedirect.com/science/article/pii/S0927025619305932
Manuscript_7d50c76e5e750081d0b6816fda96a3d8

Understanding the strain rate sensitivity of nanocrystalline copper using molecular dynamics simulations

A. Rida[a,*], M. Micoulaut[b,**], E. Rouhaud[a], A. Makke[a,c]

[a] *Laboratoire des Systèmes Mécaniques et d'Ingénierie Simultanée (LASMIS), Institut Charles Delaunay (ICD), Université de Technologie de Troyes (UTT), 10000 Troyes, France*
[b] *Laboratoire de Physique Théorique de la Matière Condensée, Paris Sorbonne Universités-UPMC, 4 Place Jussieu, 75252 Paris Cedex 05, France*
[c] *EPF, Engineering school, ERMESS Research group, 10000 Troyes, France*

Abstract

Strain rate studies of polycrystalline materials can provide information on atomic scale mechanisms in tensile strain experiments. In this work, we use molecular dynamics simulations to investigate the influence of the strain rate on the mechanical properties of nanocrystalline copper systems at a fixed average grain size (9 nm). The samples were obtained by a melting-cooling of a perfect monocrystal. A series of uniaxial tensile tests were performed at 3 orders of magnitude strain rates lower than that usually used in atomic simulations ranging from 10^4 to $10^{10} s^{-1}$ at ambient temperature. First of all, we found that the increase of the flow stress with the strain rate is caused by the delay in the onset of dislocation propagation. Furthermore, we show that while using a $\dot{\varepsilon} \geqslant 5.10^5 s^{-1}$ in atomic simulations the system is not able to reach the equilibrium state with the ongoing deformation over the ns timescale. Even in the elastic regime, the effective Young modulus of the material was found to depend on the strain rate above this threshold. In addition, The strain rate sensitivity and the flow stress activation volume are calculated, their values are consistent with experimental studies. Finally, the strain rate dependence of dislocations, twinning and grain boundaries processes is quantitatively discussed at the atomic level.

Keywords: Molecular dynamics, strain rate sensitivity, nanocrystalline copper, mechanical properties, deformation mechanism
PACS:

1. Introduction

The understanding and the prediction of the mechanical properties of nanocrystalline (NC) materials imply a detailled knowledge of the interplay between dislocation and grain boundary based deformation mechanisms [1–6]. Molecular dynamics (MD) simulations have shown that grain boundaries act as sources and sinks to dislocations in NC materials [7–12]. Swygenhoven and coworkers have shown that the nucleation and absorption of dislocations on grain boundaries i.e. Shockley partial dislocations require large grain boundary accommodation mechanisms such as atomic shuffling and stress assisted free volume migrations

*Corresponding author
**Corresponding author
Email addresses: ali.rida@utt.fr (A. Rida), mmi@lptl.jussieu.fr (M. Micoulaut)

[13–15]. Therefore, it is difficult to separate these two deformation mechanisms in order to quantify the contribution of each one to the total plastic deformation [16].

However, the sensitivity of the deformation mechanisms to the change in the imposed strain rate allows one to analyze the rate limiting of each mechanism in tension or compression tests. For example, the contribution of grain boundary sliding to plasticity was found to increase in NC materials with the decrease of the loading strain rate in NC copper tested by nanoindentation[17–19].

The study of the strain rate sensitivity of NC materials is very helpful to determine the rate limits of each deformation mechanism [20–22]. In such a way, the contribution of each deformation mechanism to the plastic deformation can be elucidated. For example, in recent MD simulations Zepeda *et al* [23] found that above a strain rate of $8.10^8\ s^{-1}$ Tantalum BCC single crystal cannot dissipate the imposed mechanical load by dislocations, however twinning becomes the dominant mechanism.

Two useful parameters can be used to quantify the degree of contribution of grain boundaries and thermally activated mechanisms to plastic deformation (i) The strain rate sensitivity (m), (ii) The activation volume (V^*). These parameters are expressed as:

$$m = \frac{\partial \ln(\sigma)}{\partial \ln(\dot{\varepsilon})} \tag{1}$$

$$V^* = \sqrt{3} k_B T \frac{\partial \ln(\dot{\varepsilon})}{\partial \sigma} \tag{2}$$

$$\Rightarrow \quad m = \frac{\sqrt{3} k_B T}{\sigma V^*} \tag{3}$$

where σ is the flow stress and $\dot{\varepsilon}$ is the strain rate, K_B being the Boltzmann constant and T the absolute temperature.

Experimental measurements of m and V^* have shown the increase of m as well as the decrease of V^* for fcc metals with the decrease of the mean grain size [17–19, 24–27]. The grain size dependence of m and V^* is interpreted by the dependence of the activation energy of dislocations on the strain rate [25]. Therefore, a small m and large V^* is measured for coarse-grained fcc metals ($\bar{d} \geq 1\mu m$) since forest lattice dislocations pileups to grain boundaries are the main deformation mechanism [28]. While the grain size decreases, the volume fraction of grain boundaries increases and hence the barriers to the motion of dislocations. Consequently, the m value increases and V^* decreases. Chen *et al* have found $m = 0.06$ and $V^* = 8b^3$ for NC copper with 10 nm mean grain size [17].

MD simulations have been used to investigate the effect of strain rate on the deformation behavior of NC fcc metals [9, 12, 29–32]. Brandl *et al* found that the flow stress decreases and cross-slip occurs frequently in NC aluminium when the strain rate decreases [31]. They suggest that at MD strain rate the grain boundaries cannot assimilate all arriving dislocations. Also, they reported that cross-slip facilitates the depining process of the full dislocation at grain boundary. Recently, inspired by experimental stress drop tests, Dupraz *et al* [9] applied a series of stress drop tests to 3D NC aluminium with 12 nm mean grain size by MD simulations. They found that at relatively low strain rates ($10^6 s^{-1}$ in MD), dislocations can propagate using low Schmid factor slip systems, a mechanism that requires a significant grain boundary assimilation processes to incorporate these dislocations.

The high strain rates commonly used in MD simulations make it however very challenging to determine the rate-limiting deformation mechanisms occurring in experiments timescale. It has been shown that the application of higher strain rates results in higher flow stresses. Under such a stress and as the grain boundaries accommodation mechanisms are mainly stress-driven [32], Brandl *et al* proposed that the dislocations are enabled to propagate athermally [31].

The strain rate dependence of the deformation mechanisms of NC materials is still not well understood. To this end, MD simulations have been employed to study the effect of the strain rate on the plastic deformation mechanisms of two columnar NC copper systems. The average grain size is 9 nm for both systems.

The strain rate used in our study varies from 10^4 to 10^{10} s^{-1}. The lowest strain rate (i.e. $\dot{\varepsilon} = 10^4$ s^{-1}) is 3 orders of magnitude lower than that usually used in MD simulations. A part of this range can be attained experimentally as in surface mechanical attrition treatment [33].

Firstly we found that at high strain rate the system falls out of equilibrium. Even in the elastic regime, the effective Young modulus of the material was found to depend on the deformation rate above a strain rate threshold ($\dot{\varepsilon} \geq 5.10^5$ s^{-1}). Our study shows an increase of the grain boundary mobility at low strain rate. The values obtained for the strain rate sensitivity and the activation volume reveal an enhancement of the grain boundaries mediated plasticity. These values are also consistent with experiments [17]. Additionally, we show in a quantitative analysis the enhancement of the twinning mechanism with the increase of the strain rate. Whereas, the nucleation of the trailing partial becomes extensive at low strain rate to form a perfect dislocation.

Our paper is organized as follows. After this introduction, we provide an overview of the methods for MD simulations in Section 2. This is followed by the results given in Section 3, which includes: (i) the strain rate dependence of the stress strain response; (ii) the influence of the strain rate on the Young modulus; and (iii) The strain rate sensitivity of the flow stress. We finalize in Section 4 with a discussion on the influence of strain rate on dislocations, twinning and grain boundaries processes and the conclusions.

2. Methods

In MD simulations, the relevance of the results depends mainly on: (i) the accuracy of the interatomic potential used and (ii) the initial configuration of the atoms. Embedded atomic method (EAM) potential developed by Foiles *et al* [34] has been used in this study. This potential describes very well the equilibrium lattice constant (a = 3.615 Å), the vacancy formation energy (1.28 eV) and the elastic constants (C_{11} = 167 GPa, C_{12} = 124 GPa, C_{44} = 76 GPa) for fcc copper metals. **The generalized stacking fault energy curve has been calculated for this potential. We found that the stacking fault energy γ_{sf} is equal to 17.8 mJ/m^2 which is somewhat lower than the experimental value[35]. However, the ratio of the stacking fault energy to the unstable stacking fault energy $\left(\frac{\gamma_{sf}}{\gamma_{usf}}\right)$ is equal to 0.15. This value is very close to that calculated by DFT [36] and for the potential of Mishin *et al* [37]. Therefore, this deficiency in the stacking fault energy will not affect the main results of the study. It should be mention that this ratio is the key factor that controles the dislocation nucleation in NC materials especially the Shockley trailing partial dislocations [38].**

A second challenge is linked with the generation of a relevant polycrystalline structure in order to model the polycrystalline materials. For instance, Voronoï tessellation is widely used to produce polycrystalline initial configurations from geometric considerations [39–41]. Another method consists of grain growth from randomly distributed initial monocrystalline seeds [42]. The major drawback in these methods is the absence of typical defects such as dislocations or vacancies inside the grains, i.e. such generated polycrystals are only an assembly of several randomly oriented perfect monocrystals. In order to compare our simulation results with the available experimental data, we have attempted to produce system with more realistic intragranular and grain boundaries structures as much as possible. For this reason, a melting cooling method has been used to produce the initial configuration as described in this reference [6]. The generated sample is a columnar NC copper system with $\bar{d}$ = 9 nm that contains 67 grains. For the same number of atoms and grain size, the columnar configurations shown here allows one to get a higher number of grains, in comparison with a cubic simulation box. This means that crystal orientations are better sampled in this kind of systems.

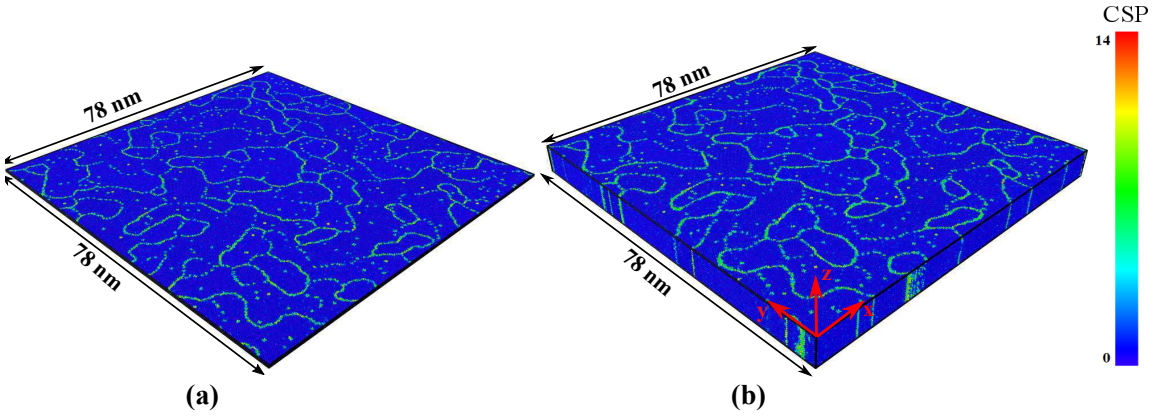

Figure 1: NC copper systems generated with the melting-cooling method. The mean grain size is 9 nm. (a) quasi-2D sample, (b) columnar 3D sample. The color of the atoms correspond to the value of their CSP: dark blue atoms are in perfect fcc position, green atoms correspond to defects or grain boundaries.

The centrosymmetric parameter (CSP) is used to characterize the microstructure [43], and defects. Atoms located in grain boundaries are identified by their higher CSP value (CSP $>$ 1 Å^2). Using CSP one can distinguish the defects from atoms with a perfect fcc position in grain interior. Thus the average grain size can be calculated. Figure 1(a) shows the atomic configuration of a quasi-2D polycrystalline sample with $\bar{d} = 9\ nm$ mapped by the CSP. The green atoms indicate the grain boundaries and the defects inside the grains that have CSP values higher than one.

For further comparison, the quasi-2D samples generated by melting quenching was then replicated fifteen times in the z direction, and relaxed in NPT ensemble at $T = 300\ K$ with zero external pressure in all directions for 200 ps. The final configuration consisted of 67 grains with mean grain size of 9 nm and 2,400,000 atoms. This method allows one to obtain a 3D columnar configuration with intragranular defects and curved grain boundaries as seen in Figure 1 (b). It is important to emphasize that this type of microstructure is commonly present in the deposition of NC thin films [44–46].

In addition to the CSP, the atomic von Mises strain is calculated based on the displacement of atoms between two configurations at different strain levels [47, 48]. The reference configuration is the initial configuration of the system. This strain is used to identify the local shear deformation which allows one to analyze the different deformation mechanisms.

The open source software "Open Visualization Tool" (OVITO) [49] is used to visualize the atomic configurations. The local crystalline structure is analyzed by adaptive common neighbor analysis [50], where fcc atoms, hcp atoms, and disordered atoms are detected and distinguished by different colors. The dislocation extraction analysis implemented in OVITO is also used to identify and determine the dislocation lines and their corresponding Burger vectors [51, 52].

To study the effect of strain rate on the mechanical properties of NC copper, uniaxial tensile tests are applied in the y direction on the quasi-2D and the columnar 3D sample. The strain rate in these tests ranges from $\dot{\varepsilon} = 10^4$ to $10^9 s^{-1}$ for the quasi-2D sample and from $\dot{\varepsilon} = 10^7$ to $10^{10} s^{-1}$ for the columnar 3D sample. The lowest strain rate for the columnar 3D sample is limited to $10^7\ s^{-1}$. Below that, the computational time becomes very large. It is also important to note that in order to reach a deformation of $\varepsilon = 0.9\%$, t_{exp} ranges from e.g. 900 ns to 9 ps from $10^4 s^{-1}$ to $10^9 s^{-1}$, respectively. The components of the pressure tensor in the x and z directions were maintained to zero during the loading. The time step used in the simulations is

3 fs. Periodic boundary conditions are applied in all directions. During the deformation, the logarithmic true strain in the tensile direction is calculated as follow:

$$ln(\lambda) = ln\left(\frac{L_y(t)}{L_y(0)}\right) \tag{4}$$

where $L_y(t)$ is the instantaneous length of the box.

The average stress tensor was computed in the y direction by using the virial stress formulation which is the sum of the kinetic energy tensor and the potential energy tensor [53, 54] :

$$\sigma_{ij}^{V} = \frac{1}{V}\sum_{\alpha}\left[\frac{1}{2}\sum_{\beta\neq\alpha}^{N}\frac{\partial U(r^{\alpha\beta})}{\partial r^{\alpha\beta}}\frac{r_i^{\alpha\beta}r_j^{\alpha\beta}}{r^{\alpha\beta}} - m^{\alpha}v_i^{\alpha}v_j^{\alpha}\right] \tag{5}$$

Where, σ_{ij}^{V} is the average component ij of the stress tensor of the system, V is the volume of the simulation box, $U(r^{\alpha\beta})$ is the atom α potential energy due to the interaction with atom β, m^{α} is the mass of atom α, and $r_j^{\alpha\beta}$ is the j^{th} component of the vector between atom α and β.

3. Results

3.1. Strain rate dependence of the stress strain response

The results of the uniaxial tensile tests applied on the NC models are presented in Figure 2. For the quasi-2D model (Figure 2 (a)) the stress increases continuously with strain to reach a threshold then fluctuates around a constant value (i.e. the flow stress). For the columnar 3D model, the stress exhibits an overshoot before the onset of the plastic flow regime. The stress strain curves in the elastic regime for the two models overlap, and the same Young's modulus is found at different strain rates (Figure 2 (c)). This indicates that the elastic response of the quasi-2D system at strain rate below $10^7\ s^{-1}$ can be extended for the columnar 3D sample.

The shape of the stress-strain curve is directly linked to the local plastic deformation mechanisms of the system. For this reason, we analyzed the atomic configurations of the systems used in this study at various strains. This allows perceiving the difference in the flow regime between the two models. We concluded that the partial dislocations mechanism is not present in the quasi-2D sample, whereas this mechanism is preponderant in the 3D samples. This justifies why the flow stress of the 3D structures is lower than that of the quasi-2D (Figure 2 (c)). For this reason, the sensitivity of the plastic deformation mechanisms to strain rate will be analyzed on the columnar 3D system. Whereas, the quasi 2D system is used to investigate the influence of the strain rate on the elastic regime due to the small size of this system and hence a lower computational power is needed.

From the stress-strain curves of the Figure 2 one can observe that:

1. The flow stress increases with respect to the strain rate.
2. There is an abrupt stress changes (i.e. jumps) in the plastic flow regime at low strain rate especially in the quasi-2D sample.
3. The overshoot of stress in columnar 3D sample becomes less pronounced when the strain rate decreases.
4. The Young's modulus depends on the applied strain rate. This indicates that the system is out of equilibrium during deformation especially at high strain rate [55].

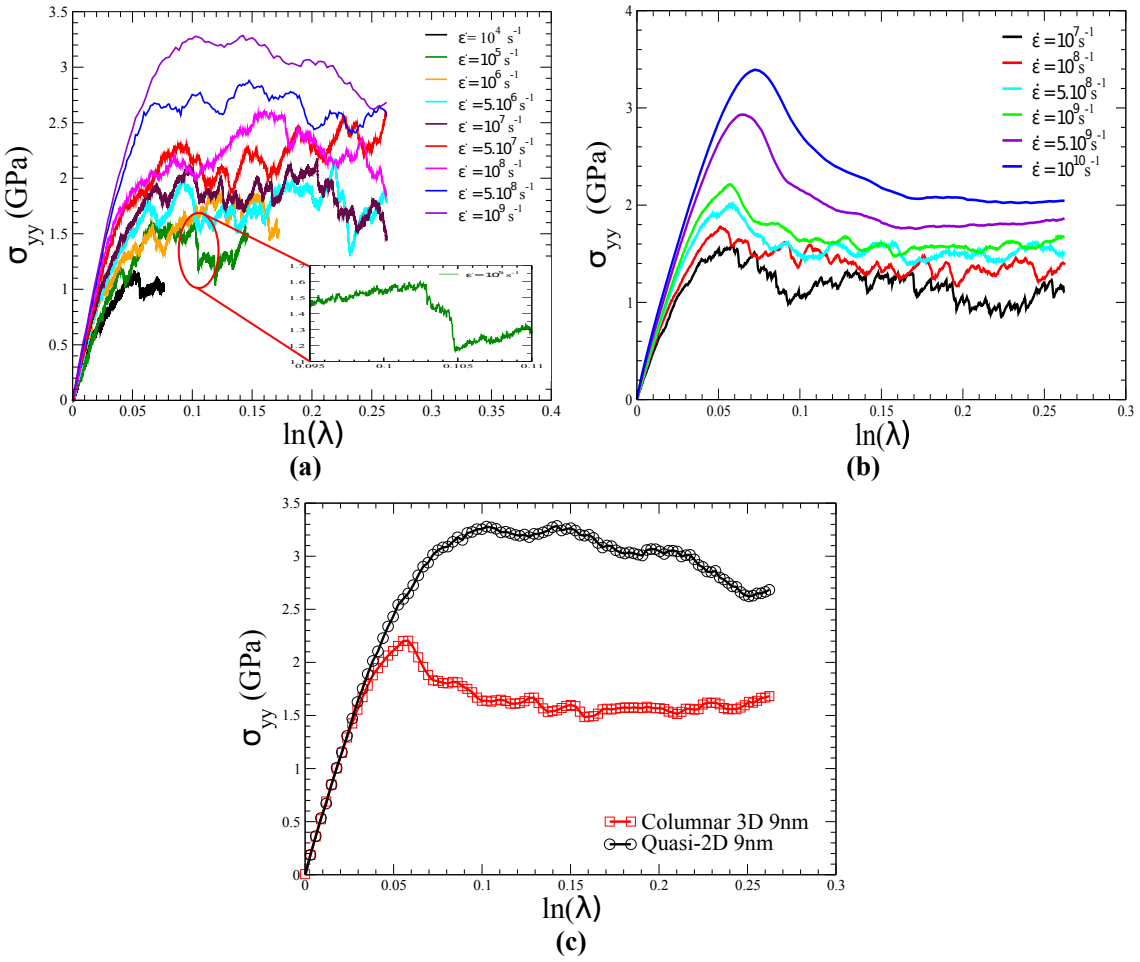

Figure 2: (a) True stress strain curves of the quasi-2D NC copper with $\bar{d} = 9\ nm$ at strain rates $\dot{\varepsilon}$ ranging from 10^4 to $10^9\ s^{-1}$. (b) True stress-strain curves of columnar 3D NC copper with $\bar{d} = 9\ nm$ at strain rates going from 10^7 to $10^{10}\ s^{-1}$. (c) Comparison of the stress-strain curves of the quasi-2D and the columnar 3D samples at $\dot{\varepsilon} = 10^9\ s^{-1}$

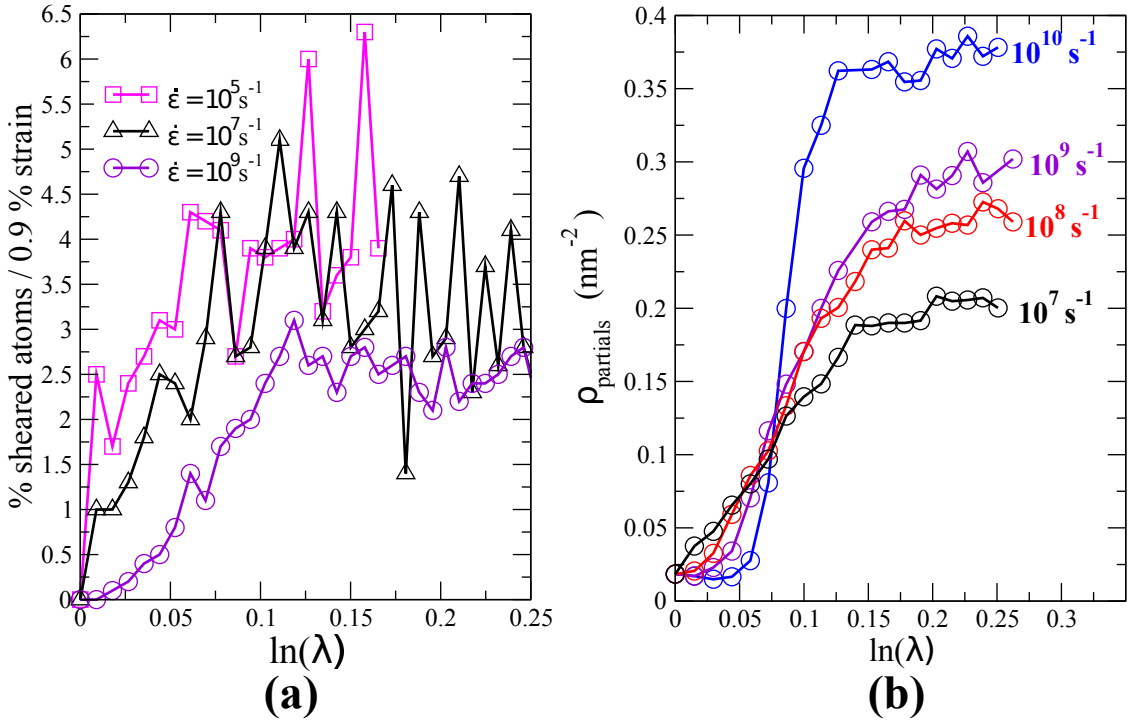

Figure 3: (a) Evolution of the fraction of sheared atoms on the sliding planes of the edge dislocations in the quasi-2D sample per 0.9% strain versus strain for different strain rates, (b) Density of the Shockley partial dislocations with $b = \frac{1}{6} < 112 >$in the columnar 3D sample versus strain for different strain rates.

The response of the macroscopic stress with respect to the increase of the applied strain depends strongly on the mobility of dislocations in the materials [56]. Therefore, the variation of the dislocation density with respect to the strain has been investigated for both models at different strain rates.

In our former work [6], we have shown that in the quasi-2D systems the emission of edge dislocations present inside the grains generates local shear bands where large shear plastic deformation is present. These dislocations move to finally vanish on the adjacent grain boundaries. Therefore, the fraction of atoms that are characterized by a high shear strain can be correlated with the density of dislocations.

To this aim, the atomic von mises strain was calculated each 0.9% strain between the actual and the reference configuration. Then the fraction of fcc atoms inside the grains having Von-Mises strain higher than 0.1 is computed. Figure 3 (a) shows the variation of the fraction of sheared atoms as a function of strain at different strain rates. This fraction increases with strain and then fluctuates around a constant value corresponding to the plastic flow regime. The increase of the fraction of sheared atoms when the strain rate decreases before the flow regime. This indicates that the onset of dislocations propagation at high strain rate is delayed which lead to an increase of the flow stress with the strain rate.

This conclusion is confirmed by the columnar 3D sample, where the Shockley partial dislocations density at different strain rates was evaluated. for this purpose the dislocation extraction analysis has been used to compute the length of all partial dislocation lines. Next, the total dislocation length is divided by the corresponding volume of the simulation box at each strain.

Figure 3 (b) shows the variation of the Shockley partial dislocations density at different strain rates. The values of our calculated dislocation densities are of the same order ($10^{17} m^{-2}$) as those found in experimental work and molecular dynamics simulations [23, 57, 58]. Two main observations can be highlighted from this Figure:

1. The density of partial dislocations for strain below 7 % decreases as the applied strain rate increases. This indicates that the delay of partial dislocations nucleation increases with the increase of the strain rate.
2. The density of partial dislocations in the flow regime increases with the strain rate (the flow regime is defined when the stress vs strain curve fluctuates around a constant value).

At high strain rate, the delay of the partial dislocations nucleation and propagation leads to a stress overshoot at yield as shown in Figure 2. Also, when the density of dislocations starts to increase the stress of the system decreases. This explains the decrease of the stress before the flow regime in Figure 2 (b). Finally, in the flow regime there is an equilibrium between the emission and annihilation of partial dislocations. As a consequence the stress remains roughly constant. This is also confirmed by the stabilization of the density of partial dislocations (Figure 3 (b)).

The inset of Figure 2 (a) shows a zoom on an abrupt drop in the flow stress at $\dot{\varepsilon} = 10^5\ s^{-1}$ between 9.5 and 11 % strain level. The analysis of the atomic configuration at these two strains show an increase of the fraction of sheared atoms from 2.7 to 3.9%. In conclusion, the change of the stress in the flow regime is directly linked to the variation of the density of dislocations. The increase of this latter induces a relaxation of the macroscopic stress by generating local plastic deformation.

3.2. Influence of strain rate on the Young modulus

For crystalline solids, the elastic regime is expected to display a Hookean behavior independent from the strain rate at ambient temperature. However, the dependence of Young's modulus on the strain rate suggests the existence of local irreversible event even in the linear regime. Young's modulus of the tested samples has been calculated from the slope of the stress-strain curve at deformation less than 0.3 %. Figure 4 shows the variation of Young's modulus as a function of the strain rate. The values of Young's modulus vary from

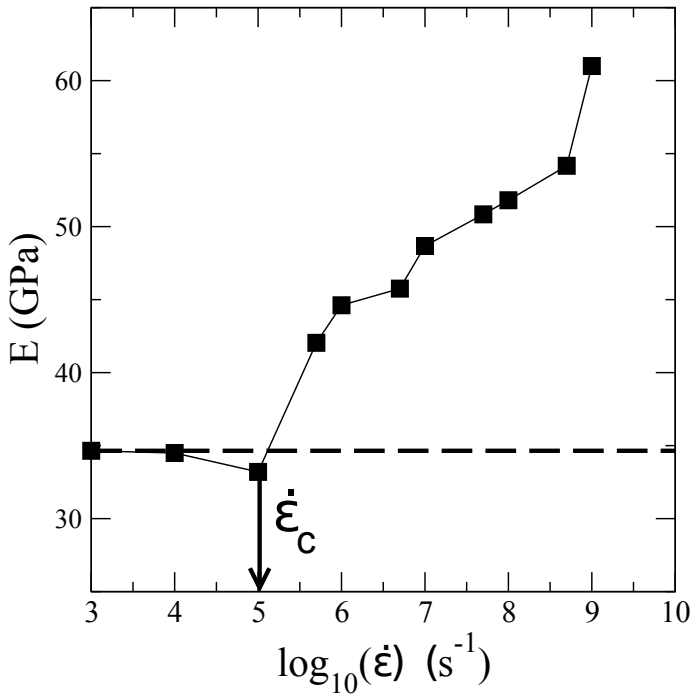

Figure 4: Variation of Young's modulus with the strain rate for the NC quasi-2D sample with 9 nm mean grain size.

35 to 61 GPa. This confirms that the elastic modulus of nanocrystalline materials is lower than their coarse grained counterparts [41, 59–61]

Interestingly, we found a threshold in Young's modulus at a strain rate of $\dot{\varepsilon}_c \simeq 5\times10^5$ s^{-1}. Below this value, Young's modulus remains nearly constant and does not depend on $\dot{\varepsilon}$, suggesting a Hookean behavior. For $\dot{\varepsilon} \geq \dot{\varepsilon}_c$, Young's modulus starts to increase with the strain rate. These results indicate that the system is not able to equilibrate above $\dot{\varepsilon}_c$ during the simulation timescale of molecular dynamics. In other words, the typical relaxation time of the material is higher than the typical timescale of the numerical experiment. Schiøtz *et al* [29] have also concluded that to completely relax the systems, strain rates must be far below what is normally used in molecular dynamics $\dot{\varepsilon} < 10^7\ s^{-1}$). The stress relaxation behavior of these models has also been investigated [55]. The results show that the stress holds constant ($\sigma(t) = \sigma_{\text{inf}}$) when a stress relaxation test is applied on configurations deformed at strain rate below $\dot{\varepsilon}_c$. This behavior is observed whatever the initial deformation level of the relaxed sample. This indicates that the system is in equilibrium state and relaxed during the simulation timescale.

3.3. Strain rate sensitivity of the flow stress

The flow stress of the samples has been calculated with respect to the strain rate. The results are shown in Figure 5, the graph (a) shows a log-log plot of the flow stress σ_f with respect to the strain rate $\dot{\varepsilon}$ for the two systems (2D and columnar 3D). As mentioned above, the flow stress increases with the strain rate. The strain rate sensitivity of the flow stress can be calculated from the slope of this log-log curve $m = \frac{\partial ln(\sigma_f)}{\partial ln(\dot{\varepsilon})}$. We find $m = 0.085$ and $m = 0.09$ for the quasi-2D and the columnar 3D samples, respectively. These results are consistent with the experimental determination of m for NC copper having similar grain size ($\approx$ 9 nm).

Chen *et al* [17] found a $m = 0.06 \pm 0.01$ for 10 nm mean grain size sample measured by nanoindentation tests. The values obtained for m are somewhat lower than those proposed for Lifshitz creep (m=1) [62] and Rachinger Grain boundary sliding (m=0.5) [63].

Figure 5 (b) displays the values of m found in the literature with respect to the mean grain size $\bar{d}$. The x axis is in logarithmic scale. Here, m increases as the grain size decreases, the values of m for the fcc NC materials being one to two orders of magnitude higher than those of the microcrystalline ones, suggesting an enhanced strain rate sensitivity for materials having $\bar{d} \leq 100\ nm$. From the strain rate sensitivity, the activation volume is computed using equation (3). We find $V^* = 2.5b^3$ for the quasi-2D system and $V^* = 3.1b^3$ for the columnar 3D one where b is the magnitude of the Burger vector. These small activation volumes in NC copper have been also measured experimentally by Chen *et al.* [17, 27]. They found $V^* = 8b^3$ for $\bar{d} = 10$ nm and $V^* = 23\ b^3$ for $\bar{d} = 42nm$. While our results are in the same order of magnitude as the experimental findings, it is important to emphasize that such small activation volumes are typical for NC materials. Indeed, for coarse-grained polycrystalline materials, the forest lattice dislocations nucleated from Frank-Read sources lead to $V^* \simeq 1000b^3$ [66]. Conversely, for nanoscale grain size such Frank-Read sources do not exist due to energetic and grain size considerations [67, 68]. However, in NC materials the grain boundaries act as sources and sinks to dislocations. Thus, the contribution of the grain boundaries mediated mechanisms to plasticity is dominating. As a result, m increases, and V^* decreases.

4. Discussion of the deformation mechanisms

In this section, the influence of the strain rate on the main deformation mechanisms of the columnar 3D model with $\bar{d} = 9nm$ will be discussed.

4.1. Influence of the strain rate on dislocations

Figure 6 shows the variation of the fraction of disordered, hcp and fcc atoms as function of the strain for different strain rates. As shown in Figure 6 (b), the fraction of hcp atoms in the flow regime increases with the strain rate. This indicates the presence of a large fraction of stacking faults hindered inside the grains at high strain rate. Therefore, partial dislocations do not have time to propagate and to be absorbed by grain boundaries at high strain rate. In consequence, the density of partial dislocation lines inside the grains will increase with the strain rate as seen in Figure 3 (b). As a result, the flow stress will increase with the strain rate.

In Figure 6 (c) the fraction of fcc atoms for the lowest strain rate $10^7 s^{-1}$ presents several abrupt jumps in the flow regime. A careful examination of the sample in this regime shows that these jumps are related to the nucleation of Shockley trailing partials to form perfect dislocations bounded by two Shockley partials. These dislocations are nucleated at high plastic strain ($ln(\lambda) \geq 10\%$) and during their propagation they eliminate the stacking fault ribbons generated by the motion of the leading partials. Hence, the fraction of fcc atoms suddenly increases. **The ratio of the stacking fault energy to the unstable stacking fault energy for the EAM copper potential is very far from 1. This indicates that the barrier to the emission of the trailing partials is very high. Also, This explains why large plastic deformation and low strain rate are needed in order to re-accumulate the stress on the grain boundaries to nucleate the trailing partials.**

When the strain rate increases these jumps disappear and the fraction of fcc atoms decreases progressively. The analysis of the atomic configurations confirms the absence of trailing partials, and instead the twinning mechanism becomes favorable. The nucleation of trailing partial is rarely seen in MD simulations of NC copper [32, 38]. However, these simulations are conducted up to 10% to 12% strain. When the strain rate decreases and the sample is deformed to larger strain, there is sufficient time to re-concentrate the stress

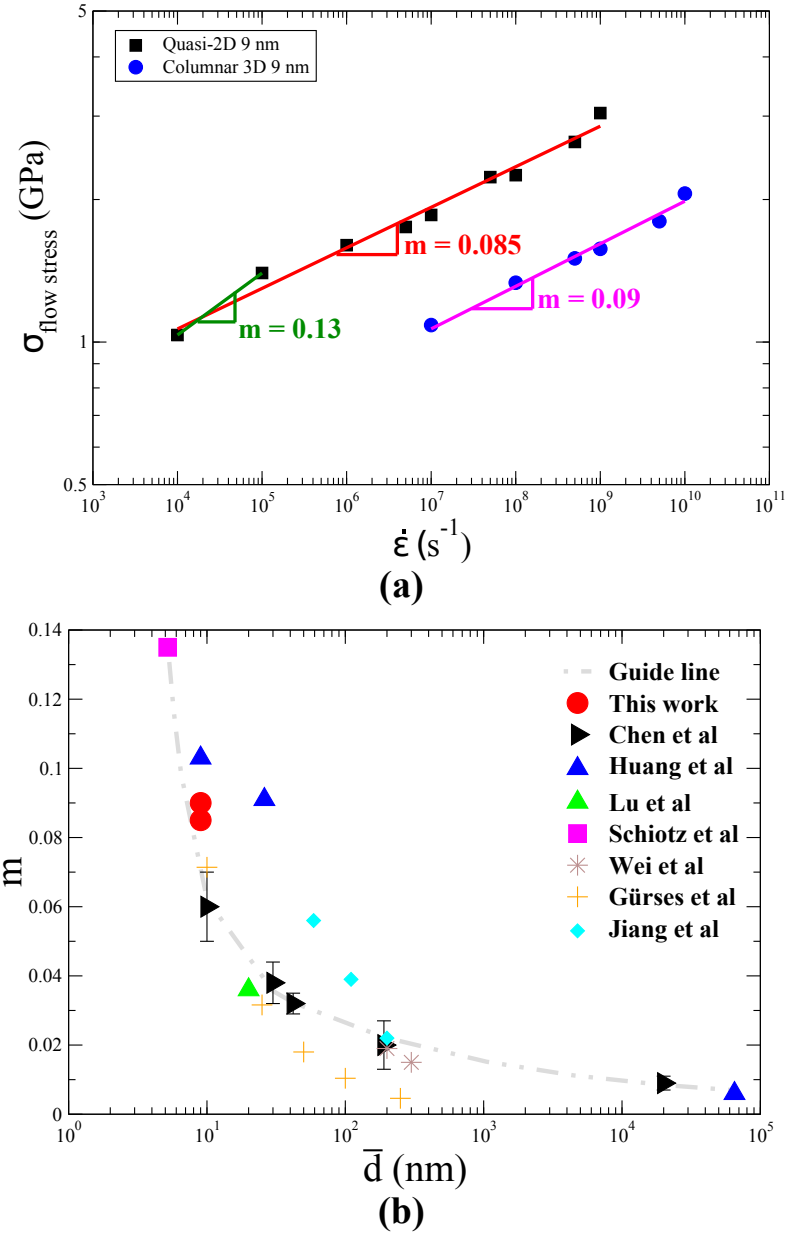

Figure 5: Log-log plot of the flow stress σ_f versus strain rate $\dot{\varepsilon}$ for the simulated NC samples having $\bar{d}$=9 nm. The slope permits one to estimate m for a fixed $\bar{d}$, (b) Variation of m as a function of the average grain size $\bar{d}$ in NC copper, compared to experimental data from the literature : Chen et al. [17], Schiøtz et al. [29], Huang et al. [19], Wei et al. [25], Lu et al. [26], Gurses et al. [64], Jiang et al [65].

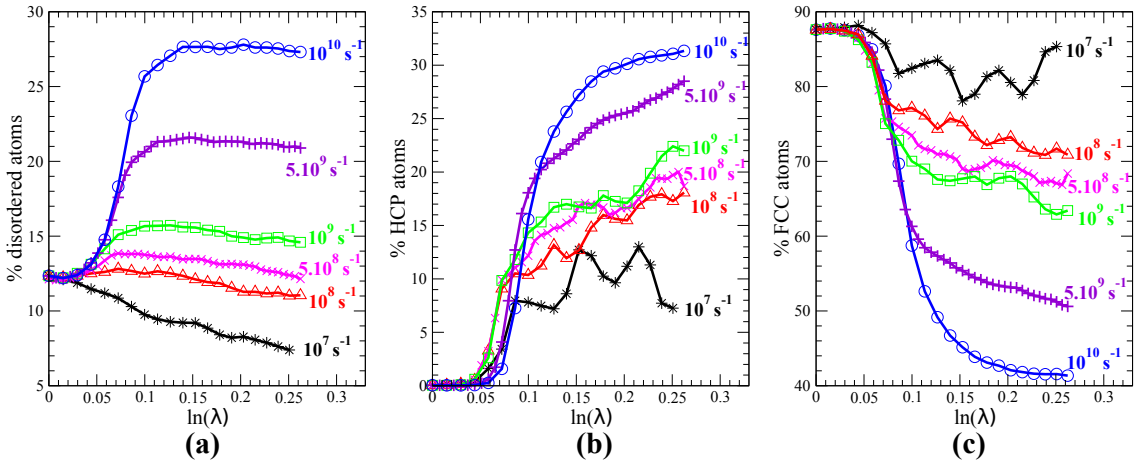

Figure 6: Fraction of atoms inside the microstructure with respect to the true strain for different tensile strain rates applied on columnar 3D NC copper sample: (a) disordered atoms, (b) hcp atoms and (c) fcc atoms.

at the grain boundaries, hence trailing partials will nucleate. For example, Zhou *et al*[69] have also seen perfect dislocations in NC copper at high strain (16%) even at $10^8 s^{-1}$. Thus, one can predict the increase of the contribution of perfect dislocations to plasticity once the strain rate decreases in NC copper down to the experimental limit.

4.2. Influence of the strain rate on twinning

The amount of twinning increases with the increase of the strain and the strain rate since the fraction of stacking faults increases (Figure 8 (b)). The presence of these faults inside the grains especially at high strain rate will increase the possibility of forming micro-twins. These micro-twins are resulting from the overlapping of the stacking faults of two partials on adjacent slip planes. This forms an extrinsic stacking fault (2 hcp planes and between them one fcc plane). Then the width of the twinned area increases with the increase of the strain by the overlapping of other dislocations on adjacent slip planes. Zhu *et al* have proposed a partial multiplication mechanism at the grain boundary in NC fcc materials that will supply a twinning partial on every successive slip plane for twin nucleation and growth [70].

Figure 7 (1) and (3) show the same two grains deformed to the same strain 16.5 % but at two different strain rates of 10^7 and 10^{10} s^{-1} respectively. As shown, the fraction of twin boundaries increases in the grain deformed at higher strain rate. The increase of the strain rate will increase the flow stress which trigger the twinning nucleation. Therefore, one can expect a transition from dislocations to twinning based mechanism with the increase of the strain rate. However, this transition is still also dependent on the grain size [71].

The total fraction of hcp atoms obtained (Figure 6 (b)) results from two main contributions: (i) twinning and (ii) partial dislocation contributions. The fraction of each part can be calculated. To quantitatively describe the influence of strain rate on twinning, the variation of the fraction of atoms in twin boundaries with strain at different strain rates has been calculated. Initially, the common neighbor analysis is applied to the system. The fcc atoms are then detected and omitted. After that, the coordination number of each atom is calculated, and the hcp atoms having a coordination number equal to six belong to twin boundaries and the rest are in stacking faults ribbons generated by the motion of partial dislocations.

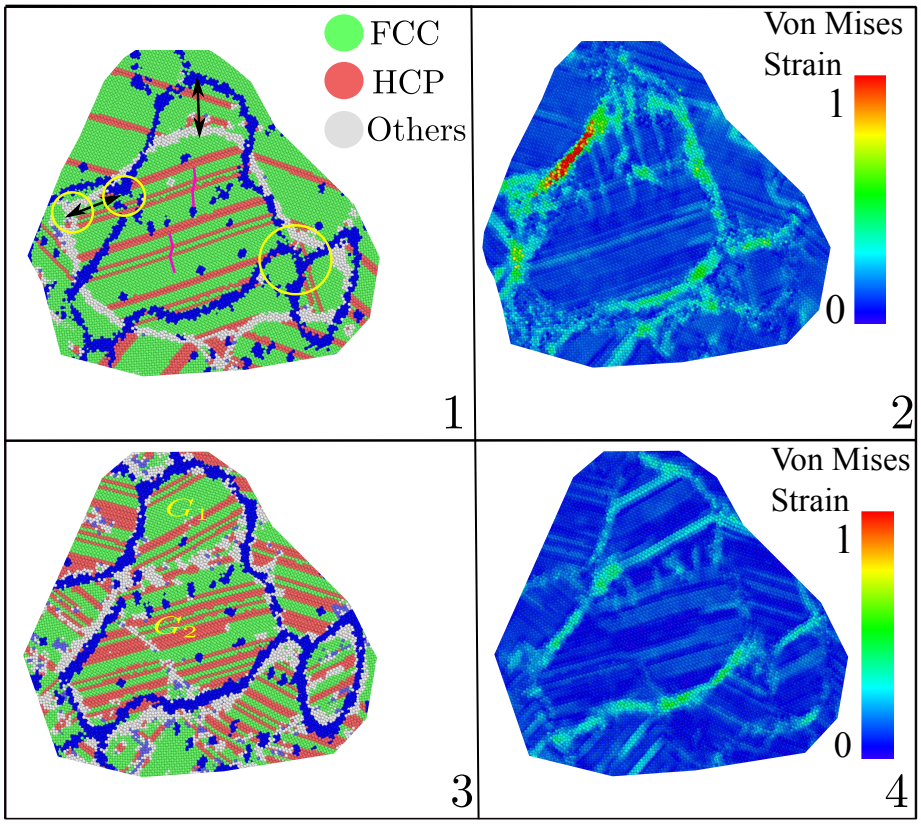

Figure 7: A zoom on two grains inside the columnar 3D sample at constant strain $ln(\lambda) = 16.5\%$ and different strain rate (1) and (2) at $10^7 s^{-1}$, (3) and (4) at $10^{10} s^{-1}$. In (1) and (2) the same grains are colored by the common neighbor analysis and the atomic Von Mises strain calculated with respect to the initial configuration at zero strain. The blue atoms in (1) are the grain boundaries of the same grains in the initial configuration, In such way the atomic processes on the grain boundaries can be detected. The snapshots (3) and (4) are respectively the same as (1) and (2) but the initial configuration is deformed at $\dot{\varepsilon} = 10^{10} s^{-1}$.

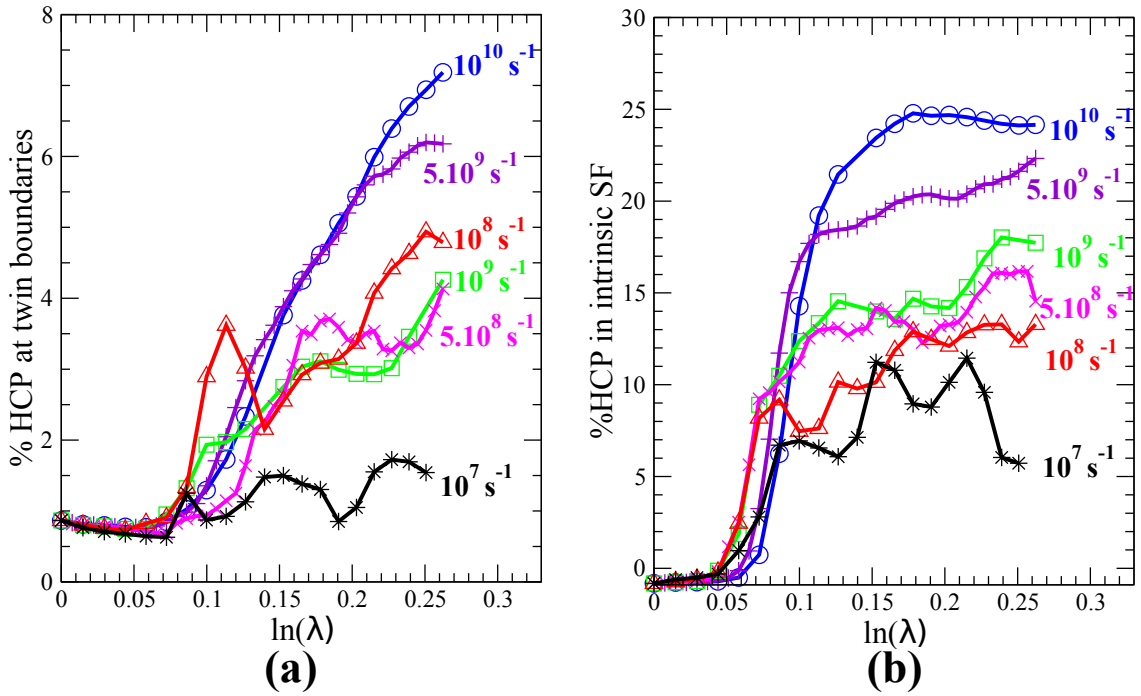

Figure 8: (a) Fraction of atoms at twin boundaries versus strain, (b) Fraction of atoms in intrinsic stacking fault ribbons generated by partial dislocations versus strain. The fraction of hcp atoms at grain boundaries increases with the strain rate. This indicates the increase of the contribution of twinning to plasticity with the strain rate.

Figure 8 (a) shows the variation of the fraction of hcp atoms in twin boundaries and in intrinsic stacking fault ribbons versus the strain for different strain rates loading. The tendency to twin increases with the strain rate (Figure 8 (a)). Also, for a strain rate of $10^7 s^{-1}$ the fraction of atoms in twin boundaries shows a small increase. This suggests that at this mean grain size the twinning mechanism is not dominant at low strain rate.

Moreover, in comparing the fraction of hcp atoms (Figure 8) the partial dislocation mechanism becomes dominant with respect to twinning, the contribution of the latter increases with the strain rate. This suggests the presence of a possible cross-over between a mechanical behavior driven by either partial dislocations or twinning. This result is consistent with a recent study[23]. Where molecular dynamics simulations is used to study the ultimate limit of metal plasticity at high strain rate. The results show that above a strain rate of $8.10^8 s^{-1}$ tantalum BCC single crystals cannot dissipate the imposed mechanical load by dislocations and twinning becomes the dominant mode of dynamic response.

4.3. Influence of the strain rate on the grain boundaries processes

The influence of the strain rate on the grain boundaries processes has been analyzed. The following observations have been noticed:

- The grain boundary and free volume migrations are enhanced with the decrease of the strain rate.
- The grain growth mechanism is limited at high strain rate.
- Even at high strain rate, in order to absorb the cores of partial dislocations in NC copper a significant amount of grain boundary activities are required to accommodate the dislocation lines at this boundary.

In Figure 7 (1) and (3) the initial grain boundaries or the defects of the grains in the initial configuration are superposed on the two snapshots and marked by blue. As shown at the lowest strain rate of 10^7 s^{-1} , one can clearly observe that the grain boundary and triple junction migrate (yellow circle and black arrows in the Figure). The atomic Von Mises strain is calculated for these deformed grains with respect to the initial configuration (Figure 7 (2)). In comparing the two figures, one can remark that large Von Mises strain is present when grain boundary and triple junction move. Also, the small grain present in the lower right region of the Figure 7 (1) collapses with the bigger grain. However, when the strain rate increases we have seen that the microstructure is roughly frozen during deformation. In Figure 7 (3) the grain boundaries in the deformed and the initial configuration overlap. Thus, the grain growth mechanisms are limited when the strain rate is high. These phenomena indicate the enhancement of the activity of grain boundary processes with reducing the strain rate especially the migrations of the grain boundaries and the triple junctions.

Figure 6 (a) shows the variation of the fraction of disordered atoms with respect to the strain at different strain rates. For $\dot{\varepsilon} > 10^8 s^{-1}$ this fraction increases up to a yield point and then becomes constant with the strain. A careful examination of the atomic configurations shows that the thickness of the grain boundaries increases with the strain rate. Thus, the barriers to the motion of dislocations become more effective. Hence the flow stress will increase with the strain rate. Zhang *et al* have also proposed that for small mean grain sizes the increase of the flow stress at higher strain rate is caused by the broadening of grain boundaries [32].

Finally, Figure 7 (4) shows the grains at 16.5% strain deformed at 10^{10} s^{-1} and colored by the atomic Von Mises strain with respect to the initial configuration. As shown, large von Mises strain is present on the grain boundaries even at such high strain rate. This indicates that the nucleation and the absorption of the partial dislocation lines required high atomic mobility on the grain boundaries. This shuffling process leads to stress relief at the grain boundaries by generating local plastic deformation. This process is consistent with the pinning-depining process proposed by Swygenhoven *et al* to explain locally how the nucleation and propagation of a perfect dislocation happen on grain boundaries in NC aluminium [13].

5. Conclusion

MD simulations have been carried out to study the effect of the strain rate on the plastic deformation of two NC copper systems, a quasi-2D and a columnar 3D one. Uniaxial tensile tests have been applied on these samples at strain rate varying from 10^4 to 10^{10} s^{-1}. The following results have been found:

- While deforming at $\dot{\varepsilon} \geqslant 5.10^5$ NC copper models are not able to relax entirely within the numerical experiment timescale at high strain rate and the system falls out of equilibrium.
- The grain boundary accommodation mechanisms are enhanced while reducing the strain rate by (i) the grain boundary and triple junction migrations and (ii) the grain growth corresponding to an increase of the strain rate sensitivity of NC copper.
- The increase of the strain rate has been found to increase the thickness of the grain boundaries and to delay the onset of dislocation nucleation and propagation resulting in an increase of the flow stress.
- At low strain rate, trailing partials have been observed at large plastic strain at a timescale of molecular dynamics.
- The contribution of twinning mechanism to plasticity increases with the strain rate but it is not the dominant deformation mechanism at this grain size even at very high strain rate ($\dot{\varepsilon} = 10^{10}$ s^{-1}).

It should be certainly interesting to investigate how the grain size affects the present sensitivity to the strain rate in nanocrystalline copper. Work in this direction is in progress.

6. Acknowledgments

The authors gratefully acknowledge the financial supports for this work provided by European FEDER funds and the Région Grand-Est. This work was further supported by the French HPC Center ROMEO.

[1] T. J. Rupert, Strain localization in a nanocrystalline metal: Atomic mechanisms and the effect of testing conditions, Journal of applied physics 114 (3) (2013) 033527.

[2] J. R. Trelewicz, C. A. Schuh, The hall–petch breakdown in nanocrystalline metals: a crossover to glass-like deformation, Acta Materialia 55 (17) (2007) 5948–5958.

[3] Y. Zhang, G. J. Tucker, J. R. Trelewicz, Stress-assisted grain growth in nanocrystalline metals: Grain boundary mediated mechanisms and stabilization through alloying, Acta Materialia 131 (2017) 39–47.

[4] A. Kobler, C. Brandl, H. Hahn, C. Kübel, In situ observation of deformation processes in nanocrystalline face-centered cubic metals, Beilstein journal of nanotechnology 7 (2016) 572.

[5] G. J. Tucker, S. M. Foiles, Quantifying the influence of twin boundaries on the deformation of nanocrystalline copper using atomistic simulations, International Journal of Plasticity 65 (2015) 191–205.

[6] A. Rida, E. Rouhaud, A. Makke, M. Micoulaut, B. Mantisi, Study of the effects of grain size on the mechanical properties of nanocrystalline copper using molecular dynamics simulation with initial realistic samples, Philosophical Magazine 97 (27) (2017) 2387–2405.

[7] H. Van Swygenhoven, Grain boundaries and dislocations, Science 296 (5565) (2002) 66–67.

[8] H. Van Swygenhoven, J. R. Weertman, Deformation in nanocrystalline metals, Materials today 9 (5) (2006) 24–31.

[9] M. Dupraz, Z. Sun, C. Brandl, H. Van Swygenhoven, Dislocation interactions at reduced strain rates in atomistic simulations of nanocrystalline al, Acta Materialia 144 (2018) 68–79.

[10] J. Schiøtz, T. Vegge, F. D. Di Tolla, K. W. Jacobsen, Atomic-scale simulations of the mechanical deformation of nanocrystalline metals, Phys. Rev. B 60 (1999) 11971–11983.

[11] V. Yamakov, D. Wolf, S. Phillpot, A. Mukherjee, H. Gleiter, Deformation mechanism crossover and mechanical behaviour in nanocrystalline materials, Philosophical Magazine Letters 83 (6) (2003) 385–393.

[12] J. Schiøtz, K. W. Jacobsen, A maximum in the strength of nanocrystalline copper, Science 301 (5638) (2003) 1357–1359.

[13] H. Van Swygenhoven, P. Derlet, A. Frøseth, Nucleation and propagation of dislocations in nanocrystalline fcc metals, Acta Materialia 54 (7) (2006) 1975–1983.

[14] A. Frøseth, P. Derlet, H. Van Swygenhoven, Dislocations emitted from nanocrystalline grain boundaries: nucleation and splitting distance, Acta Materialia 52 (20) (2004) 5863–5870.

[15] H. Van Swygenhoven, P. Derlet, A. Hasnaoui, Atomic mechanism for dislocation emission from nanosized grain boundaries, Physical Review B 66 (2) (2002) 024101.

[16] N. Vo, R. Averback, P. Bellon, S. Odunuga, A. Caro, Quantitative description of plastic deformation in nanocrystalline cu: Dislocation glide versus grain boundary sliding, Physical Review B 77 (13) (2008) 134108.

[17] J. Chen, L. Lu, K. Lu, Hardness and strain rate sensitivity of nanocrystalline cu, Scripta Materialia 54 (11) (2006) 1913–1918.

[18] S. Cheng, E. Ma, Y. Wang, L. Kecskes, K. Youssef, C. Koch, U. Trociewitz, K. Han, Tensile properties of in situ consolidated nanocrystalline cu, Acta materialia 53 (5) (2005) 1521–1533.

[19] P. Huang, F. Wang, M. Xu, K. Xu, T. Lu, Dependence of strain rate sensitivity upon deformed microstructures in nanocrystalline cu, Acta Materialia 58 (15) (2010) 5196–5205.

[20] S. Van Petegem, S. Brandstetter, B. Schmitt, H. Van Swygenhoven, Creep in nanocrystalline ni during x-ray diffraction, Scripta Materialia 60 (5) (2009) 297–300.

[21] R. S. Kottada, A. H. Chokshi, Low temperature compressive creep in electrodeposited nanocrystalline nickel, Scripta materialia 53 (8) (2005) 887–892.

[22] A. H. Chokshi, Unusual stress and grain size dependence for creep in nanocrystalline materials, Scripta Materialia 61 (1) (2009) 96–99.

[23] L. A. Zepeda-Ruiz, A. Stukowski, T. Oppelstrup, V. V. Bulatov, Probing the limits of metal plasticity with molecular dynamics simulations, Nature 550 (7677) (2017) 492.

[24] D. Gianola, D. Warner, J.-F. Molinari, K. Hemker, Increased strain rate sensitivity due to stress-coupled grain growth in nanocrystalline al, Scripta Materialia 55 (7) (2006) 649–652.

[25] Q. Wei, S. Cheng, K. Ramesh, E. Ma, Effect of nanocrystalline and ultrafine grain sizes on the strain rate sensitivity and activation volume: fcc versus bcc metals, Materials Science and Engineering: A 381 (1-2) (2004) 71–79.

[26] L. Lu, S. Li, K. Lu, An abnormal strain rate effect on tensile behavior in nanocrystalline copper, Scripta Materialia 45 (10) (2001) 1163–1169.

[27] J. Chen, Y. Shi, K. Lu, Strain rate sensitivity of a nanocrystalline cu–ni–p alloy, Journal of materials research 20 (11) (2005) 2955–2959.

[28] Mechanical properties of nanocrystalline materials, Progress in Materials Science 51 (4) (2006) 427 – 556.

[29] J. Schiøtz, F. D. Di Tolla, K. W. Jacobsen, Softening of nanocrystalline metals at very small grain sizes, Nature 391 (6667) (1998) 561.

[30] J. Schiøtz, T. Vegge, F. Di Tolla, K. W. Jacobsen, Atomic-scale simulations of the mechanical deformation of nanocrystalline metals, Physical Review B 60 (17) (1999) 11971.

[31] C. Brandl, P. M. Derlet, H. Van Swygenhoven, Strain rates in molecular dynamics simulations of nanocrystalline metals, Philosophical Magazine 89 (34-36) (2009) 3465–3475.

[32] T. Zhang, K. Zhou, Z. Chen, Strain rate effect on plastic deformation of nanocrystalline copper investigated by molecular dynamics, Materials Science and Engineering: A 648 (2015) 23–30.

[33] J. Azadmanjiri, C. C. Berndt, A. Kapoor, C. Wen, Development of surface nano-crystallization in alloys by surface mechanical attrition treatment (smat), Critical Reviews in Solid State and Materials Sciences 40 (3) (2015) 164–181.

[34] S. Foiles, M. Baskes, M. S. Daw, Embedded-atom-method functions for the fcc metals cu, ag, au, ni, pd, pt, and their alloys, Physical review B 33 (12) (1986) 7983.

[35] S. Ogata, J. Li, S. Yip, Ideal pure shear strength of aluminum and copper, Science 298 (5594) (2002) 807–811.

[36] J. A. Zimmerman, H. Gao, F. F. Abraham, Generalized stacking fault energies for embedded atom fcc metals, Modelling and Simulation in Materials Science and Engineering 8 (2) (2000) 103.

[37] C. Brandl, Deformation mechanism in nanocrystalline fcc metals studied by atomistic simulations.

[38] H. Van Swygenhoven, P. Derlet, A. Frøseth, Stacking fault energies and slip in nanocrystalline metals, Nature materials 3 (6) (2004) 399.

[39] P. Hirel, Atomsk: a tool for manipulating and converting atomic data files, Computer Physics Communications 197 (2015) 212–219.

[40] A. Okabe, B. Boots, K. Sugihara, S. N. Chiu, Spatial tessellations: concepts and applications of Voronoi diagrams, Vol. 501, John Wiley & Sons, 2009.

[41] G.-J. J. Gao, Y.-J. Wang, S. Ogata, Studying the elastic properties of nanocrystalline copper using a model of randomly packed uniform grains, Computational Materials Science 79 (2013) 56–62.

[42] B. Mantisi, Generation of polycrystalline material at the atomic scale, Computational Materials Science 118 (2016) 245–250.

[43] C. L. Kelchner, S. Plimpton, J. Hamilton, Dislocation nucleation and defect structure during surface indentation, Physical review B 58 (17) (1998) 11085.

[44] M.-S. Colla, B. Amin-Ahmadi, H. Idrissi, L. Malet, S. Godet, J.-P. Raskin, D. Schryvers, T. Pardoen, Dislocation-mediated relaxation in nanograined columnar palladium films revealed by on-chip time-resolved hrtem testing, Nature communications 6 (2015) 5922.

[45] H. Gong, J. Hu, J. Wang, C. Ong, F. Zhu, Nano-crystalline cu-doped zno thin film gas sensor for co, Sensors and Actuators B: Chemical 115 (1) (2006) 247–251.

[46] P. Barna, M. Adamik, Fundamental structure forming phenomena of polycrystalline films and the structure zone models, Thin solid films 317 (1-2) (1998) 27–33.

[47] F. Shimizu, S. Ogata, J. Li, Theory of shear banding in metallic glasses and molecular dynamics calculations, Materials transactions 48 (11) (2007) 2923–2927.

[48] M. Falk, J. Langer, Dynamics of viscoplastic deformation in amorphous solids, Physical Review E 57 (6) (1998) 7192.

[49] A. Stukowski, Visualization and analysis of atomistic simulation data with ovito–the open visualization tool, Modelling and Simulation in Materials Science and Engineering 18 (1) (2009) 015012.

[50] A. Stukowski, A. stukowski, modell. simul. mater. sci. eng. 18, 015012 (2010)., Modell. Simul. Mater. Sci. Eng. 18 (2010) 015012.

[51] A. Stukowski, K. Albe, Extracting dislocations and non-dislocation crystal defects from atomistic simulation data, Modelling and Simulation in Materials Science and Engineering 18 (8) (2010) 085001.

[52] A. Stukowski, V. V. Bulatov, A. Arsenlis, Automated identification and indexing of dislocations in crystal interfaces, Modelling and Simulation in Materials Science and Engineering 20 (8) (2012) 085007.

[53] S. Plimpton, Fast parallel algorithms for short-range molecular dynamics, Journal of computational physics 117 (1) (1995) 1–19.

[54] A. K. Subramaniyan, C. Sun, Continuum interpretation of virial stress in molecular simulations, International Journal of Solids and Structures 45 (14-15) (2008) 4340–4346.

[55] A. Rida, M. Micoulaut, E. Rouhaud, A. Makke, Crystals at high deformation rates displaying glassy behavior, physica status solidi (b) (2019) 1800649.

[56] J. P. Hirth, J. Lothe, Theory of dislocations.

[57] R. Cotterill, Does dislocation density have a natural limit?, Physics Letters A 60 (1) (1977) 61–62.

[58] X. Liao, Y. Zhao, S. Srinivasan, Y. Zhu, R. Valiev, D. Gunderov, Deformation twinning in nanocrystalline copper at room temperature and low strain rate, Applied physics letters 84 (4) (2004) 592–594.

[59] P. G. Sanders, J. Eastman, J. Weertman, Elastic and tensile behavior of nanocrystalline copper and palladium, Acta materialia 45 (10) (1997) 4019–4025.

[60] P. Valat-Villain, J. Durinck, P. Renault, Grain size dependence of elastic moduli in nanocrystalline tungsten, Journal of Nanomaterials 2017.

[61] G. Nieman, J. Weertman, R. Siegel, Mechanical behavior of nanocrystalline cu and pd, Journal of Materials Research 6 (5) (1991) 1012–1027.

[62] R. Coble, A model for boundary diffusion controlled creep in polycrystalline materials, Journal of applied physics 34 (6) (1963) 1679–1682.

[63] H. Lüthy, R. A. White, O. D. Sherby, Grain boundary sliding and deformation mechanism maps, Materials Science and Engineering 39 (2) (1979) 211–216.

[64] E. Gürses, T. El Sayed, Constitutive modeling of strain rate effects in nanocrystalline and ultrafine grained polycrystals, International Journal of Solids and Structures 48 (10) (2011) 1610–1616.

[65] Y. Jiang, J. Hu, Z. Jiang, J. Lian, C. Wen, Strain rate dependence of tensile strength and ductility of nano and ultrafine grained coppers, Materials Science and Engineering: A 712 (2018) 341–349.

[66] R. Abbaschian, R. E. Reed-Hill, Physical metallurgy principles, Cengage Learning, 2008.

[67] T. Nieh, J. Wadsworth, Hall-petch relation in nanocrystalline solids, Scripta Metallurgica et Materialia 25 (4) (1991) 955–958.

[68] P. Derlet, H. Van Swygenhoven, A. Hasnaoui, Atomistic simulation of dislocation emission in nanosized grain boundaries, Philosophical Magazine 83 (31-34) (2003) 3569–3575.

[69] K. Zhou, B. Liu, Y. Yao, K. Zhong, Effects of grain size and shape on mechanical properties of nanocrystalline copper investigated by molecular dynamics, Materials Science and Engineering: A 615 (2014) 92–97.

[70] Y. Zhu, X. Wu, X. Liao, J. Narayan, S. Mathaudhu, L. Kecskes, Twinning partial multiplication at grain boundary in nanocrystalline fcc metals, Applied Physics Letters 95 (3) (2009) 031909.

[71] X. Wu, Y. Zhu, Inverse grain-size effect on twinning in nanocrystalline ni, Physical review letters 101 (2) (2008) 025503.

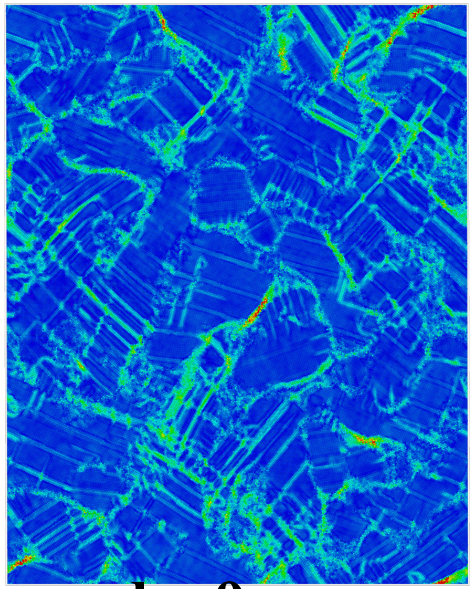

d = 9nm

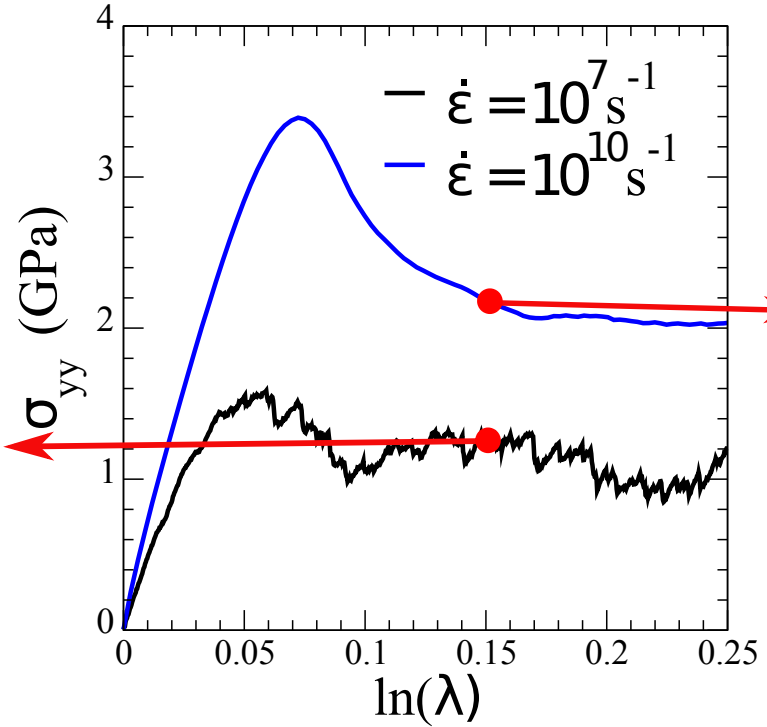
$\dot{\varepsilon} = 10^{7}\,s^{-1}$
$\dot{\varepsilon} = 10^{10}\,s^{-1}$
σ_{yy} (GPa)
ln(λ)
0
1
2
3
4
0
0.05
0.1
0.15
0.2
0.25

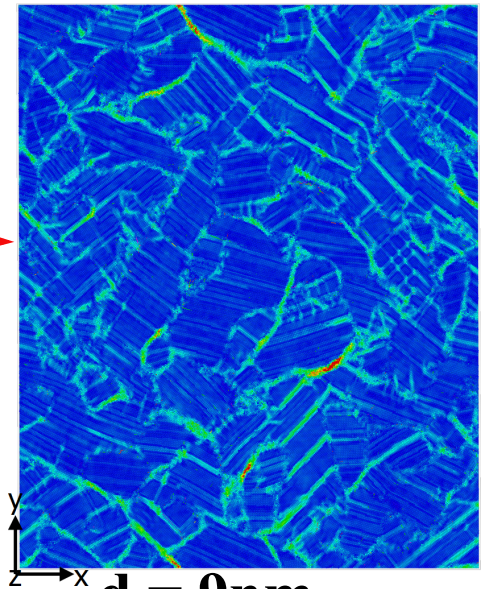
y
z
x

d = 9nm


Von Mises
Strain
1
0